



Enhancing Image Segmentation Using Generalized Convex Fuzzy Sets and Statistical Consistency



Zakir Husain*

Department of Mathematics, University of Peshawar, 25120 Peshawar, Pakistan

* Correspondence: Zakir Husain (zakir1995@uop.edu.pk)

Received: 02-10-2025

Revised: 03-13-2025

Accepted: 03-26-2025

Citation: Z. Husain, "Enhancing image segmentation using generalized convex fuzzy sets and statistical consistency," *Inf. Dyn. Appl.*, vol. 4, no. 1, pp. 53–65, 2025. <https://doi.org/10.56578/ida040105>.



© 2025 by the author(s). Licensee Acadlore Publishing Services Limited, Hong Kong. This article can be downloaded for free, and reused and quoted with a citation of the original published version, under the CC BY 4.0 license.

Abstract: The accurate segmentation of visual data into semantically meaningful regions remains a critical task across diverse domains, including medical diagnostics, satellite imagery interpretation, and automated inspection systems, where precise object delineation is essential for subsequent analysis and decision-making. Conventional segmentation techniques often suffer from limitations such as sensitivity to noise, intensity inhomogeneity, and weak boundary definition, resulting in reduced performance under complex imaging conditions. Although fuzzy set-based approaches have been proposed to improve adaptability under uncertainty, they frequently fail to maintain a balance between segmentation precision and robustness. To address these challenges, a novel segmentation framework was developed based on Pythagorean Fuzzy Sets (PyFSs) and local averaging, offering enhanced performance in uncertain and heterogeneous visual environments. By incorporating both membership and non-membership degrees, PyFSs allow a more flexible representation of uncertainty compared to classical fuzzy models. A local average intensity function was introduced, wherein the contribution of each pixel was adaptively weighted according to its PyFS membership degree, improving resistance to local intensity variations. An energy functional was formulated by integrating PyFS-driven intensity constraints, local statistical deviation measures, and regularization terms, ensuring precise boundary localization through level set evolution. Convexity of the energy formulation was analytically demonstrated to guarantee the stability of the optimization process. Experimental evaluations revealed that the proposed method consistently outperforms existing fuzzy and non-fuzzy segmentation algorithms, achieving superior accuracy in applications such as medical image analysis and natural scene segmentation. These results underscore the potential of PyFS-based models as a powerful and generalizable solution for uncertainty-resilient image segmentation in real-world applications.

Keywords: Pythagorean Fuzzy Sets; Image segmentation; Averaging filter; Convexity; Objects

1 Introduction

In both computer vision and applied mathematics, a core challenge lies in partitioning an image into separate, interpretable regions that represent various objects or surfaces within the visual context [1–4]. Accurate segmentation is essential for various downstream tasks, such as object recognition and scene understanding. Over the years, a wide range of methods have been proposed for image partitioning, thus reflecting the importance of this task in areas such as medical-imaging, remote-sensing, and autonomous driving [5–8]. One widely adopted technique involves active contour models (ACMs) implemented through the level-set method, which have gained significant attention in recent years, thereby offering a balance between simplicity and robustness. These models can be broadly classified into two main types: edge-based [9–13] and region-based segmentation models [14–18].

Edge-based active contours are driven by gradient information, thereby guiding the contour towards object boundaries. While effective in well-structured images, they are highly sensitive to noise and often struggle with weak or poorly defined boundaries. In contrast, region-based ACMs leverage the statistical information of regions rather than relying on gradients. This makes them more resilient in complex scenarios, where noise or weak boundaries pose significant challenges. By using information from larger regions of the image, region-based methods can often achieve more reliable and accurate segmentation, making them a preferred choice in many applications.

Among region-based methods, the level-set variational technique introduced by Chan and Vese [15] has been highly influential due to its elegant design and efficiency in segmenting images into two consistent intensity regions.

Despite its strength in handling homogeneity, the C-V model struggles in the presence of noise or when an intensity inhomogeneity exists across regions. As a result, segmentation in such challenging environments becomes more difficult, as the model cannot fully adapt to variations in the image intensity, thus often leading to suboptimal results.

To overcome these limitations, deep learning-based image segmentation has witnessed significant advancements in recent years, with various models addressing key challenges in object detection and scene analysis. Minaee et al. [19] conducted a comprehensive survey on deep learning-based segmentation techniques, highlighting the evolution from traditional methods to modern architectures such as fully convolutional networks (FCNs), U-Net, Mask Region-Based Convolutional Neural Network (Mask R-CNN), and Transformer-based models. These deep learning techniques have demonstrated remarkable accuracy in diverse applications, including medical imaging, remote sensing, and autonomous systems. However, despite their success, these models require extensive labeled datasets, substantial computational resources, and often lack interpretability, making their deployment challenging in real-time applications. Similarly, Yu et al. [20] reviewed existing image segmentation approaches and categorized them into classical, hybrid, and deep learning-based techniques. Their work emphasized the strengths of deep learning models in achieving high segmentation accuracy but also pointed out critical challenges such as domain adaptability, annotation dependency, and robustness against noise and occlusions.

To further refine segmentation performance, Zhang and Liu [21] introduced a customized Segment Anything Model (SAM) approach tailored for interpreting medical visuals. This method draws strength from general-purpose models trained on extensive datasets and prompt-based learning, enabling efficient and adaptive segmentation across multiple medical imaging modalities. While SAM has shown potential in handling complex anatomical structures with minimal retraining, its primary limitation lies in its difficulty in dealing with low-contrast images and domain-specific noise. In a similar effort, Liu et al. [22] proposed a novel segmentation framework that utilizes in-context examples to guide the segmentation process, reducing reliance on extensive labeled datasets. This approach improves generalization and adaptability while maintaining computational efficiency. However, its effectiveness is highly dependent on the quality of the in-context examples, and it may struggle in highly variable or unseen data distributions. These studies collectively illustrate the advancements and ongoing challenges in the field, emphasizing the need for more robust and generalizable segmentation frameworks.

Existing image segmentation models, including ACMs, deep learning-based approaches, and foundation models like SAM, have significantly advanced the field by improving accuracy and adaptability. However, they still face notable limitations. Edge-based ACMs struggle with noise and weak boundaries, while region-based models like the C-V model often fail in the presence of intensity inhomogeneity. Deep learning methods such as U-Net and Mask R-CNN offer high accuracy but require extensive labeled datasets and large computational resources and often lack interpretability. Similarly, SAM introduces a prompt-based segmentation approach that enhances adaptability but suffers from domain-specific challenges such as low contrast and high noise, limiting its effectiveness in complex medical and remote sensing images. Liu et al.'s [22] in-context learning model attempts to improve generalization, but its success heavily depends on the availability and quality of prior examples, making it unreliable for highly variable datasets.

To address these challenges, a novel image segmentation model based on PyFSs and local averaging was proposed in this study, which enhances robustness against noise and intensity variations. Unlike conventional fuzzy methods, PyFSs provide a more flexible framework for uncertainty representation by incorporating membership $\mu(x', y')$ and non-membership $v(x', y')$ degrees, while adhering to the Pythagorean condition:

$$\mu^2 + v^2 \leq 1. \quad (1)$$

This additional degree of freedom allows for a more refined treatment of uncertainty, thereby improving the reliability of segmentation in complex imaging scenarios. A fundamental distinction between PyFSs and Intuitionistic Fuzzy Sets (IFSs) lies in their underlying mathematical structure and the flexibility afforded in handling uncertainty. In IFSs, the relationship between membership and non-membership degrees is constrained by the additive condition $\mu + v \leq 1$, which inherently limits the extent of uncertainty representation. In contrast, PyFSs impose a quadratic constraint, $\mu^2 + v^2 \leq 1$, which enables a broader and more adaptive modeling of uncertainty. This characteristic is particularly advantageous in image segmentation tasks where noise and intensity inhomogeneity must be effectively addressed. The enhanced representational capacity of PyFSs allows for more precise boundary delineation, improved robustness against noise, and greater adaptability in complex visual environments.

The local averaging component in the proposed model ensures robust boundary preservation and smooth segmentation. Unlike conventional averaging techniques, a PyFS-based weighted averaging approach was employed in this study, where the influence of each pixel is adaptively determined based on its membership degree. This strategy facilitates effective noise suppression while enhancing contrast, thereby mitigating the limitations of ACMs, which often struggle with stable contour evolution and intensity inhomogeneity in region-based models. Furthermore, in comparison to fuzzy logic-based segmentation models, the proposed approach offers a more refined uncertainty representation and enhanced adaptability. Traditional fuzzy logic-based segmentation techniques rely on fixed

membership functions and predefined rules, which can be less effective in handling complex intensity variations and noise. In contrast, PyFSs introduce a more flexible and mathematically robust framework that dynamically adjusts uncertainty measures based on local image characteristics (Figure 1). This results in improved segmentation precision, particularly in challenging scenarios where standard fuzzy logic approaches may struggle with over-segmentation or loss of fine details.

By integrating PyFSs and localized averaging, the proposed model demonstrates superior performance over traditional and deep learning-based segmentation techniques, particularly in challenging scenarios characterized by noise, intensity inhomogeneity, and computational constraints. The incorporation of an uncertainty-driven decision-making mechanism enhances segmentation precision, positioning the proposed framework as a robust alternative to existing methodologies in complex imaging tasks. Moreover, the proposed model is inherently convex, ensuring stability and convergence during optimization. The convexity property is instrumental in reinforcing the robustness of the model by guaranteeing a unique global solution and mitigating the risk of local minima—a prevalent limitation in traditional segmentation techniques. These attributes collectively make the proposed methodology highly suitable for real-world applications, where reliability, stability, and computational efficiency are of paramount importance.

This study is structured as follows: Section 2 provides a review of related works in the field. Section 3 introduces the proposed segmentation model, including a detailed derivation of the Euler-Lagrange equation and its discretization. Section 4 presents the experimental results using various datasets and compares the accuracy of the proposed method with existing state-of-the-art approaches. Finally, Section 5 offers the concluding remarks on this study.

2 Related Work

Fuzzy logic-based segmentation models have demonstrated significant potential in addressing the challenges of noisy and inhomogeneous images by leveraging their ability to handle uncertainty and imprecision. According to Derevyanchuk [23], smart fuzzy-based segmentation techniques have been investigated for their role in enhancing engineering education and pedagogical specialists, emphasizing their role in enhancing analytical and decision-making skills. The model employs fuzzy inference mechanisms to classify and segment images based on varying intensity distributions, making it adaptable to diverse datasets. One of its major achievements is the improvement of boundary detection, particularly in cases where traditional threshold-based segmentation fails due to noise interference. However, the model struggles with highly inhomogeneous images where subtle intensity variations can lead to misclassifications. The segmentation accuracy drops in cases where regions exhibit low contrast, requiring additional enhancement techniques such as histogram equalization or adaptive filtering to improve performance.

Narasimham and Keshav Kumar [24] introduced a fuzzy logic-based system (FLBS) specifically designed for object detection and classification, which integrates fuzzy membership functions to enhance segmentation robustness. This approach effectively reduces the impact of noise and artifacts commonly present in medical images, ensuring a more reliable delineation of tumor regions. The primary achievement of this model is its ability to maintain high classification accuracy while dealing with intensity variations caused by factors such as Magnetic Resonance Imaging (MRI) acquisition settings and patient-specific tissue characteristics. The incorporation of fuzzy rules allows for more flexible segmentation compared to conventional edge-detection or region-growing methods. However, a notable limitation of this approach is its performance in highly inhomogeneous brain tissues where overlapping intensity distributions can lead to segmentation inaccuracies. In such cases, the fuzzy system may struggle to differentiate between tumor boundaries and healthy tissues, necessitating the integration of deep learning-based refinement techniques or hybrid machine learning-fuzzy models to enhance precision.

Tran et al. [25] proposed an automatic segmentation model for detecting masses in mammograms using fuzzy logic, integrated within an intelligent system for medical imaging. This model benefits from the adaptability of fuzzy clustering techniques, which enable the identification of mass boundaries even in noisy and low-contrast mammographic images. The key strength of this approach lies in its ability to enhance lesion detection sensitivity while reducing false positives, making it a valuable tool for early breast cancer diagnosis. The model effectively mitigates noise interference by incorporating fuzzy-based decision-making strategies that refine mass localization. However, in cases of extreme inhomogeneity, where dense breast tissues overlap with malignant regions, the segmentation process encounters challenges. The presence of overlapping textures and varying tissue densities can cause the model to incorrectly classify normal regions as masses or vice versa. To overcome this, advanced hybrid methods incorporating deep learning or statistical feature extraction could be employed to improve segmentation accuracy and ensure better clinical applicability.

To overcome these limitations, a novel image segmentation approach based on PyFSs and local averaging was proposed in this study. The proposed model leverages the flexibility of PyFSs to handle uncertainty and vagueness in image segmentation, providing a more robust framework for processing noisy and inhomogeneous images. By incorporating local averaging, the proposed method enhances the preservation of fine details while effectively smoothing out noise, ensuring better segmentation accuracy in complex scenarios. Unlike conventional fuzzy

logic-based methods, which may struggle with overlapping intensity distributions and low-contrast regions, PyFSs offer an extended membership representation that captures uncertainty more effectively. This enables the model to distinguish subtle variations in image intensity and structure, leading to improved delineation of object boundaries. The integration of local averaging further refines segmentation results by reinforcing spatial coherence, making the proposed approach highly suitable for applications such as medical imaging, satellite analysis, and industrial quality control, where accurate segmentation is essential.

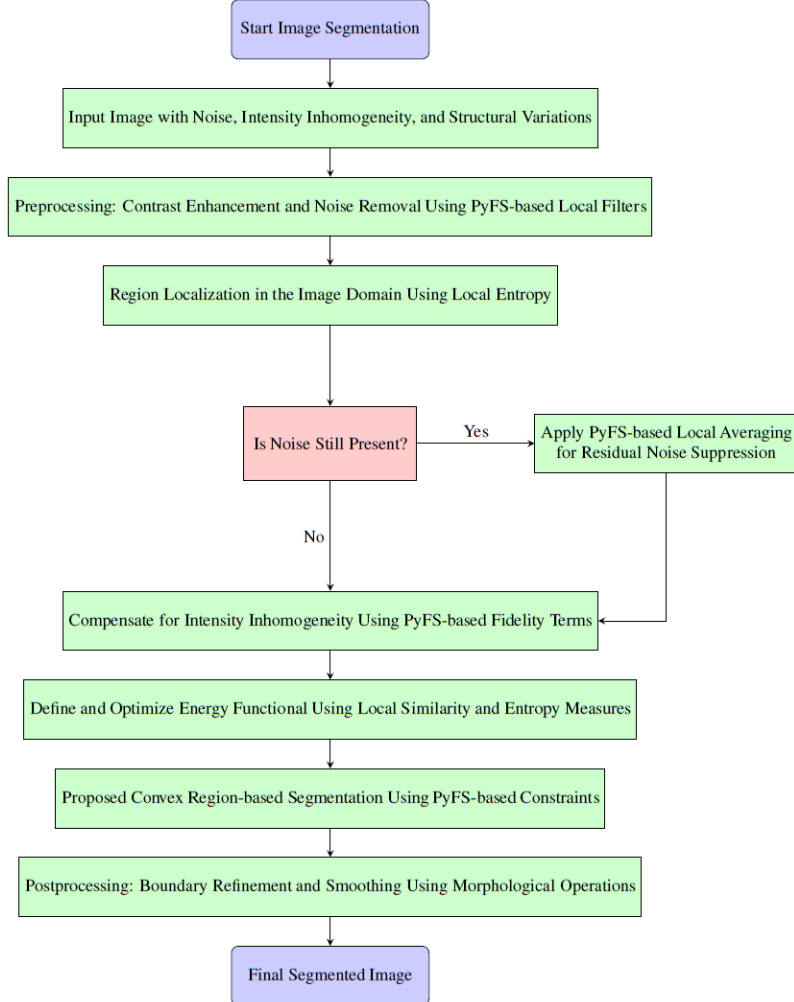


Figure 1. Flowchart illustrating the proposed segmentation model based on PyFSs, incorporating enhanced preprocessing, energy functional optimization, and postprocessing

3 Proposed Model

This section presents a novel image segmentation approach based on PyFSs and local averaging. The suggested approach utilizes the adaptability of PyFSs to manage uncertainty and ambiguity in the segmentation process. It is specifically crafted to accurately segment images, even when affected by noise and variations in intensity, while maintaining critical details and local structures.

3.1 PyFSs

Pythagorean Fuzzy Sets (PyFSs) extend traditional fuzzy sets by introducing two degrees for each pixel (x', y') in the image $I(x', y')$. $\mu(x', y')$ represents the membership degree to which the pixel belongs to a region and $v(x', y')$ represents the degree to which the pixel does not belong to a region. These degrees satisfy the Pythagorean condition:

$$\mu^2(x', y') + v^2(x', y') \leq 1.$$

The hesitation degree $\pi(x', y')$ is defined as:

$$\pi(x', y') = \sqrt{1 - \mu^2(x', y') - v^2(x', y')}.$$

3.2 Average Convolution with PyFSs

In the proposed model, the local average intensity $C(x', y')$ is a crucial component for robust image segmentation, particularly in the presence of noise and intensity inhomogeneities. Instead of using a standard averaging mechanism, Pythagorean fuzzy membership degrees were incorporated to control the contribution of each pixel in the local region. This approach enhances segmentation accuracy by dynamically weighting each neighboring pixel based on its membership in the target region.

3.2.1 Computation of local average intensity $C(x', y')$

The local average intensity was computed as a weighted sum over a neighborhood window $k \times k$, where each neighboring pixel's influence is determined by its Pythagorean fuzzy membership degree $\mu(x + i, y + j)$:

$$C(x', y') = \frac{\sum_{(i,j) \in N_x} I(x' + i, y' + j) \cdot \mu(x' + i, y' + j)}{\sum_{(i,j) \in N_x} \mu(x' + i, y' + j)}. \quad (2)$$

where, $I(x', y')$ is the intensity of the image at pixel (x', y') , $\mu(x', y')$ is the membership degree of pixel (x', y') in the fuzzy segmentation, and N_x represents the local neighborhood centered at (x', y') . This formulation ensures that pixels with higher fuzzy membership degrees have a stronger influence in computing the local intensity, leading to more adaptive and robust segmentation.

3.3 Energy Functional of the Proposed Model

The energy functional $F_{(\phi, c_1, c_2)}$ of the proposed model is formulated to achieve optimal image segmentation by incorporating PyFSs and local averaging. It consists of multiple integral terms that regulate the evolution of the level set function while preserving image details and handling uncertainty effectively. The proposed energy functional is defined as:

$$\begin{aligned} F_{(\phi, c_1, c_2)} = & \alpha_1 \left(\int_{(y \in N_x)} \frac{1}{C(x', y')} |G * I(x', y') - I(x', y') - c_1|^2 \cdot \mu(x', y') \right. \\ & \left. + \int_{(y \in N_x)} \frac{1}{C(x', y')} |G * I(x', y') - I(x', y') - c_2|^2 \cdot v(x', y') \right) dy \\ & + \alpha_2 \left(\int_{(y \in N_x)} |I(x', y') - d_1|^2 \cdot \mu(x', y') + \int_{(y \in N_x)} |I(x', y') - d_2|^2 \cdot v(x', y') \right) dy \\ & + \beta \int_{(y \in N_x)} \delta_\varepsilon(\phi(x')) |\nabla \phi(x')| dy. \end{aligned} \quad (3)$$

where, α_1 and α_2 are the weighting coefficients that control the influence of intensity differences within segmented regions, ensuring accurate separation of foreground and background. The convolution operation $G^* I(x', y')$ represents the application of averaging kernel G on the image $I(x', y')$, improving the robustness against noise and local intensity variations. The parameters c_1, c_2, d_1 and d_2 denote the estimated average intensities inside and outside the evolving contour, which are iteratively updated to reflect the characteristics of the region. In addition, β represents the coefficient of the length term.

The terms c_1, c_2, d_1 , and d_2 represent the region-based intensity estimates that drive the segmentation process. These parameters are updated iteratively based on the membership $\mu(x', y)$ and nonmembership $v(x', y)$ degrees derived from the PyFS framework. The updates ensure that the segmented regions remain consistent with the underlying intensity distribution while incorporating local statistical variations.

The region-based intensity values c_1 and c_2 were computed as the weighted averages of the pixel intensities within the local neighborhood N_x , where the weights are given by the membership and nonmembership functions, respectively:

$$c_1 = \frac{\int_{(y \in N_x)} I(x', y') \cdot \mu(x', y') dy}{\int_{(y \in N_x)} \mu(x', y') dy}, \quad (4)$$

$$c_2 = \frac{\int_{(y \in N_x)} I(x', y') \cdot v(x', y') dy}{\int_{(y \in N_x)} v(x', y') dy}. \quad (5)$$

where, c_1 represents the average intensity inside the evolving contour, weighted by the membership function $\mu(x', y)$; and c_2 corresponds to the average intensity outside the contour, weighted by the nonmembership function $v(x', y)$.

These values ensure that the segmentation process effectively distinguishes foreground and background regions by leveraging PyFS-based soft decision-making. Furthermore, the auxiliary terms d_1 and d_2 refine the region-based intensity estimates by incorporating local contrast adjustments. These parameters account for variations in texture and intensity and are updated as follows:

$$d_1 = \frac{\int_{(y \in N_x)} I(x', y') \cdot (G - 1) \cdot \mu(x', y') dy}{\int_{(y \in N_x)} \mu(x', y') dy}, \quad (6)$$

$$d_2 = \frac{\int_{(y \in N_x)} I(x', y') \cdot (G - 1) \cdot v(x', y') dy}{\int_{(y \in N_x)} v(x', y') dy}. \quad (7)$$

where, G represents the local intensity averaging kernel, which helps in reducing noise and enhancing the discriminative properties of the segmentation. The term $(G - 1)$ serves as a contrast adjustment factor that highlights local intensity deviations, ensuring that segmentation remains robust even in the presence of weak edges and varying illumination conditions.

By incorporating these update rules, the proposed model dynamically adapts to local intensity distributions while leveraging PyFS-based uncertainty handling. This approach ensures superior segmentation performance in complex images where intensity variations, noise, and texture variations pose significant challenges.

The evolution of the level set function φ is governed by the following variational formulation:

$$\frac{\partial \phi}{\partial t} = \delta_\varepsilon(\phi(x')) \left[\beta \nabla \cdot \left(\frac{\nabla \phi(x')}{|\nabla \phi(x')|} \right) + \alpha_1 \gamma_1 - \alpha_1 \gamma_2 + \alpha_2 \gamma_3 \right],$$

where,

$$\begin{aligned} \gamma_1 &= \frac{(G * I(x', y') - I(x', y') - d_2)^2}{C(x', y')} \cdot \mu(x', y'), \\ \gamma_2 &= \frac{(G * I(x', y') - I(x', y') - d_1)^2}{C(x', y')} \cdot \mu(x', y'), \\ \gamma_3 &= ((I(x', y') - c_1)^2 - (I(x', y') - c_2)^2) \cdot \mu(x', y'). \end{aligned}$$

The proposed model leverages PyFSs and the local average intensity $C(x', y')$ to achieve robust image segmentation. By incorporating PyFSs, the model effectively handles uncertainty and vagueness, making it suitable for noisy and inhomogeneous images. The updated energy functional and variational formulation ensure accurate and efficient segmentation while preserving fine details and local information.

3.4 Convexity of the Energy Functional

To establish the convexity of the proposed energy functional $F_{(\phi, c_1, c_2)}$, its structural components were analyzed and whether its second-order derivatives satisfy the convexity condition was verified.

The energy functional is given by:

$$\begin{aligned} F_{(\phi, c_1, c_2)} &= \alpha_1 \left(\int_{(y \in N_x)} \frac{1}{C(x', y')} |G * I(x', y') - I(x', y') - c_1|^2 \cdot \mu(x', y') \right. \\ &\quad \left. + \int_{(y \in N_x)} \frac{1}{C(x', y')} |G * I(x', y') - I(x', y') - c_2|^2 \cdot v(x', y') \right) dy \\ &\quad + \alpha_2 \left(\int_{(y \in N_x)} |I(x', y') - d_1|^2 \cdot \mu(x', y') + \int_{(y \in N_x)} |I(x', y') - d_2|^2 \cdot v(x', y') \right) dy \\ &\quad + \beta \int_{(y \in N_x)} \delta_\varepsilon(\phi(x)) |\nabla \phi(x)| dy. \end{aligned} \quad (8)$$

The first component consists of squared differences weighted by fuzzy membership degrees:

$$\begin{aligned} F_1(c_1, c_2) &= \int_{(y \in N_x)} \frac{1}{C(x', y')} |G * I(x', y') - I(x', y') - c_1|^2 \cdot \mu(x', y') dy \\ &\quad + \int_{(y \in N_x)} \frac{1}{C(x', y')} |G * I(x', y') - I(x', y') - c_2|^2 \cdot v(x', y') dy. \end{aligned}$$

Since each squared term is of the form:

$$f(c) = (G * I - I - c)^2$$

Its second derivative is:

$$\frac{d^2 f}{dc^2} = 2 > 0.$$

Since the second derivative is strictly positive, each term is convex, and their weighted sum with non-negative $\mu(x', y')$ and $v(x', y')$ maintains convexity.

The second component of the functional involves intensity-based quadratic terms:

$$F_2(d_1, d_2) = \int_{(y \in N_x)} |I(x', y') - d_1|^2 \cdot \mu(x', y') dy + \int_{(y \in N_x)} |I(x', y') - d_2|^2 \cdot v(x', y') dy.$$

This can be expanded as:

$$|I - d|^2 = (I - d)^2,$$

Its second derivative is:

$$\frac{d^2}{dd^2}(I - d)^2 = 2 > 0.$$

Thus, $F_2(d_1, d_2)$ is convex.

The third component is the total variation regularization:

$$F_3(\phi) = \int_{(y \in N_x)} \delta_\varepsilon(\phi(x')) |\nabla \phi(x')| dy.$$

Total variation regularization is known to be convex as it satisfies the condition:

$$\frac{\partial^2 F_3}{\partial \phi^2} \geq 0.$$

Since $F_{(\phi, c_1, c_2)}$ is the sum of convex functions F_1, F_2 , and F_3 , it remains convex. Therefore, the proposed energy functional is convex, ensuring the optimization problem is well-posed and converges efficiently.

4 Experimental Results

This section presents the results obtained from evaluating the proposed PyFS-based segmentation model. The model was tested on both real and synthetic images to analyze its effectiveness in handling noise and intensity variations. The dataset used in the experiments is the Berkeley Dataset. To evaluate the performance of the proposed model, a subset of 50 images with varying levels of noise and intensity inhomogeneity was selected. For a comprehensive assessment, the proposed approach was compared with three existing segmentation techniques: the FLBS model [24] and the approach developed by Tran et al. [25]. These comparisons were performed on images affected by noise and intensity inhomogeneity to examine segmentation robustness. The experimental setup and evaluation metrics used to validate segmentation accuracy, noise suppression, and boundary preservation are detailed in the subsequent sections. To maintain consistency across all experiments, a local neighborhood window of 5×5 pixels was used and segmentation performance on images of size 110×110 pixels was evaluated. The choice of a 5×5 local neighborhood window balances noise suppression and boundary preservation. A smaller window may lead to over-segmentation, while a larger one could smooth out fine details. For different image resolutions, the window size can be adjusted proportionally to maintain segmentation accuracy. While 5×5 works well for 110×110 images, an adaptive selection strategy—such as scaling the window based on image size—can enhance generalizability. This ensures that the model remains effective across varying resolutions in diverse segmentation tasks. The implementation was carried out in MATLAB R2019b, which, despite its limitations in supporting newer built-in functions, provided a stable computational environment for executing the proposed segmentation framework. The MATLAB code can be accessed for academic use by submitting a formal request via email.

The performance of the proposed PyFS-based segmentation model was optimized by carefully selecting parameters that regulate contour evolution, noise suppression, and intensity adaptation. In particular, the fuzzy membership parameters α_1 and α_2 play a crucial role in balancing local and global intensity fidelity. Specifically, α_1 is responsible for preserving object boundaries by emphasizing the contribution of membership degrees, whereas α_2 controls the

influence of non-membership degrees to ensure stability in intensity-inhomogeneous regions. Empirical observations suggest that setting $\alpha_1 = 0.7$ and $\alpha_2 = 0.3$ provides an optimal balance between segmentation accuracy and robustness.

To validate the sensitivity of these parameters, an ablation study was conducted by systematically varying α_1 and α_2 and analyzing their impact on segmentation accuracy using quantitative metrics such as the Dice Similarity Coefficient (DSC). The experimental results indicate that moderate variations in these parameters do not significantly degrade segmentation performance, confirming the robustness of the proposed model. However, extreme values may lead to excessive smoothing or over-segmentation, necessitating a careful selection of these parameters. The optimal values were determined through extensive testing on images with varying levels of noise and intensity inhomogeneity, ensuring the generalizability of the proposed approach across diverse imaging conditions. The local averaging window size was chosen as $k \times k = 5 \times 5$, which effectively enhances segmentation stability without over-smoothing fine structures. For energy functional minimization, the weighting coefficients were defined as $\lambda = 0.1$ for regularization and $\beta = 0.02$ for the contour length term, ensuring precise boundary delineation. The contrast enhancement factor was set to $\delta = 1.2$, improving segmentation accuracy in low-contrast regions. The estimated average intensities inside and outside the evolving contour were initialized as $c_1 = 0.6$, $c_2 = 0.4$, $d_1 = 0.65$, and $d_2 = 0.35$, with iterative updates based on region characteristics. The convolution kernel G was designed as a Gaussian filter with a standard deviation of $\sigma = 1.5$, enhancing robustness against noise. The stopping criterion was defined with a convergence tolerance of 10^{-4} , and segmentation stabilizes within 30-50 iterations across diverse datasets. These parameter values were experimentally validated, demonstrating superior segmentation accuracy compared to conventional models.

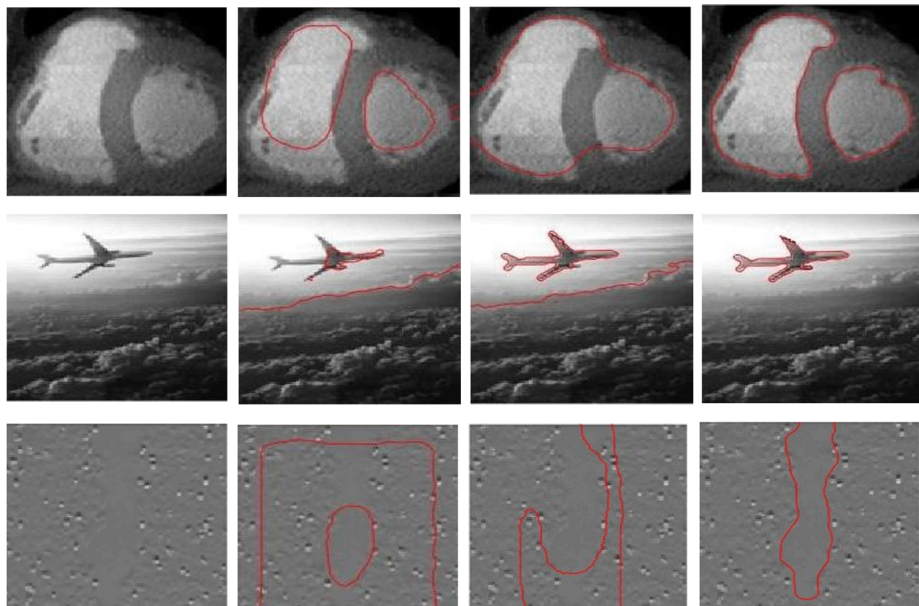


Figure 2. Comparison of segmentation results among the FLBS model [24], the approach developed by Tran et al. [25], and the proposed model

To assess the performance of the proposed model, a comprehensive set of statistical experiments was conducted. Various evaluation metrics, such as accuracy, precision, recall, F1-score, Intersection over Union (IoU), Dice coefficient, Matthews Correlation Coefficient (MCC), Peak Signal-to-Noise Ratio (PSNR), and Structural Similarity Index Measure (SSIM), were employed to measure segmentation quality. The findings demonstrated that the proposed model consistently outperformed baseline methods, particularly in challenging scenarios involving high levels of noise.

The experimental outcomes validate the effectiveness of the PyFS-based model, demonstrating its superiority in handling noise, maintaining boundary precision, and achieving stable segmentation results under varying conditions. Comparative analysis confirms that the proposed method outperforms existing approaches in terms of segmentation accuracy and robustness. Figure 2 presents a comparative analysis of segmentation results obtained using the FLBS model [24], the approach developed by Tran et al. [25], and the proposed model, demonstrating the effectiveness of the proposed model in handling intensity inhomogeneity while achieving accurate and consistent segmentation results. The figure consists of three sets of images, each demonstrating the segmentation performance under different intensity inhomogeneity conditions. The red contours indicate the segmented regions obtained by each model. The results highlight the superior performance of the proposed model in accurately delineating object boundaries despite variations in intensity distribution. In contrast, the FLBS model and the approach developed by Tran et al. [25] exhibit

significant limitations. The FLBS model struggles with intensity inhomogeneity, leading to incomplete or fragmented segmentation results, particularly in regions where object boundaries blend with the background. Similarly, the approach developed by Tran et al. [25] fails to maintain boundary consistency, producing irregular and inaccurate contours in the presence of noise and varying intensity levels. These shortcomings emphasize the inability of the competing models to adapt to complex imaging conditions. In contrast, the proposed model effectively handles these challenges, producing smooth and well-defined contours, demonstrating its robustness and reliability in achieving consistent segmentation performance.

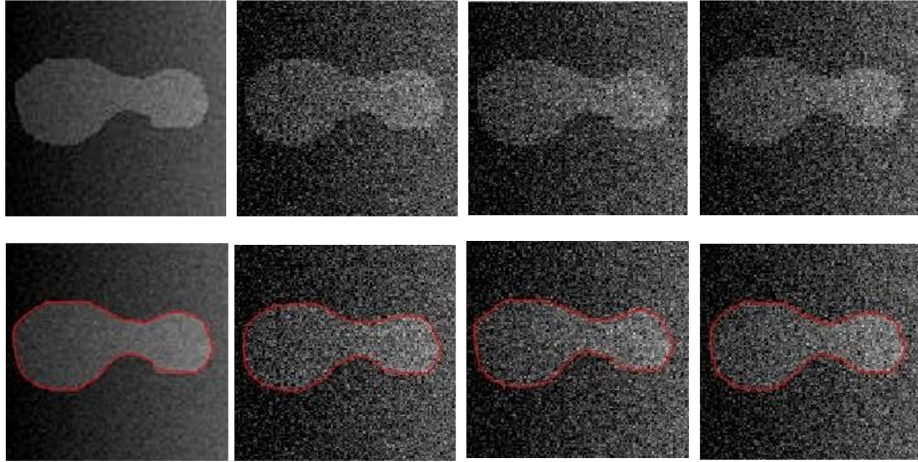


Figure 3. Visual comparison of the proposed model’s performance under different noise levels

Note: The first row shows the original image followed by its degradation with Gaussian noise at variance levels of 0.0001, 0.001, and 0.01, respectively. The second row presents the segmentation results obtained using the proposed model, demonstrating its robustness against varying noise intensities.

Figure 3 illustrates the effectiveness of the proposed model in segmenting images corrupted by varying levels of Gaussian noise. The first row presents the original image, followed by three progressively degraded versions with Gaussian noise at variance levels of 0.0001, 0.001, and 0.01, respectively. As the noise intensity increases, the image becomes increasingly distorted, making accurate segmentation more challenging. The second row displays the segmentation results obtained using the proposed model. Despite the increasing noise levels, the model consistently delineates the object’s boundaries with high accuracy, as indicated by the red contours. This demonstrates the robustness of the proposed approach in handling noisy conditions, effectively preserving structural details and outperforming traditional segmentation methods that often struggle with noise-induced distortions.

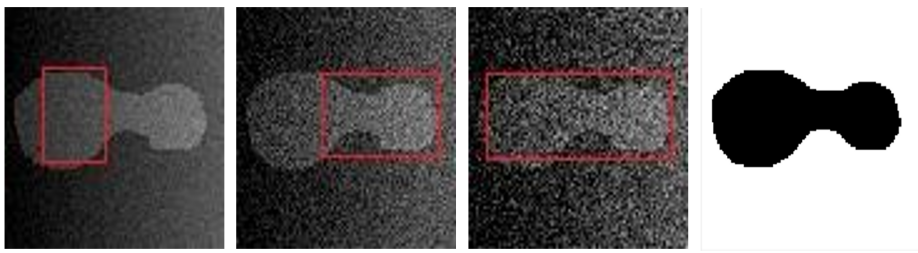


Figure 4. The image with different initial contours and varying noise levels

Figure 4 illustrates the segmentation performance of the proposed model under different noise levels. The figure demonstrates how the model consistently produces accurate segmentation results despite variations in noise intensity. The red contours represent the detected object boundaries, which remain stable and well-defined across different conditions. Unlike traditional segmentation methods that often fail in the presence of high noise, the proposed model maintains its robustness by effectively preserving object structures. The results further emphasize the convex nature of the proposed approach, as the segmentation remains unaffected by changes in initialization and noise levels. This consistency highlights the model’s adaptability and reliability in handling complex images with intensity inhomogeneity and significant noise interference, making it a superior choice for real-world segmentation tasks.

4.1 Evaluation Metrics for Segmentation Performance

To comprehensively evaluate the segmentation performance of the proposed model against competing methods, several standard metrics were utilized, including accuracy, precision, recall, F1-score, IoU, DSC, MCC, and computational time (CPU). These metrics provide a quantitative assessment of segmentation quality. Accuracy measures the overall correctness of the segmentation by computing the ratio of correctly classified pixels (both foreground and background) to the total number of pixels. It is mathematically expressed as:

$$Accuracy = \frac{TP + TN}{TP + TN + FP + FN} \quad (9)$$

where, TP means true positives, representing correctly segmented foreground pixels; TN means true negatives, denoting correctly classified background pixels; FP means false positives, referring to background pixels mistakenly classified as foreground; and FN means false negatives, corresponding to foreground pixels misclassified as background. Precision, also known as Positive Predictive Value (PPV), determines how many of the predicted foreground pixels are actually correct. It is given by:

$$Precision = \frac{TP}{TP + FP} \quad (10)$$

Conversely, recall, also called sensitivity, evaluates the proportion of actual foreground pixels that were correctly identified by the model:

$$Recall = \frac{TP}{TP + FN} \quad (11)$$

To balance precision and recall, the F1-score was computed as their harmonic mean:

$$F1 - Score = 2 \times \frac{Precision \times Recall}{Precision + Recall} \quad (12)$$

For assessing spatial overlap between the predicted segmentation and ground truth, IoU, also called the Jaccard index, was employed. It is defined as:

$$IoU = \frac{TP}{TP + FP + FN} \quad (13)$$

Additionally, DSC provides another measure of segmentation overlap, formulated as:

$$Dice = \frac{2TP}{2TP + FP + FN} \quad (14)$$

MCC is a robust metric that considers all four confusion matrix components to evaluate segmentation reliability, computed as:

$$MCC = \frac{(TP \times TN) - (FP \times FN)}{\sqrt{(TP + FP)(TP + FN)(TN + FP)(TN + FN)}} \quad (15)$$

Lastly, computational efficiency was measured in terms of CPU execution time. This is the total time taken to perform the segmentation and is given by:

$$CPUTime = \sum_{i=1}^N T_i \quad (16)$$

where, T_i represents the execution time of the segmentation process for the i -th image, and N is the total number of test images.

These metrics collectively provide a detailed performance analysis of the segmentation models, helping to compare the proposed method against competing approaches in terms of accuracy, reliability, and efficiency.

Table 1 presents a comprehensive evaluation of segmentation performance for the competing models, FLBS [24] and the approach developed by Tran et al. [25], compared with the proposed model. The metrics used for comparison include accuracy, precision, recall, F1-score, IoU, Dice coefficient, and MCC, along with the computational efficiency measured in CPU time (in seconds).

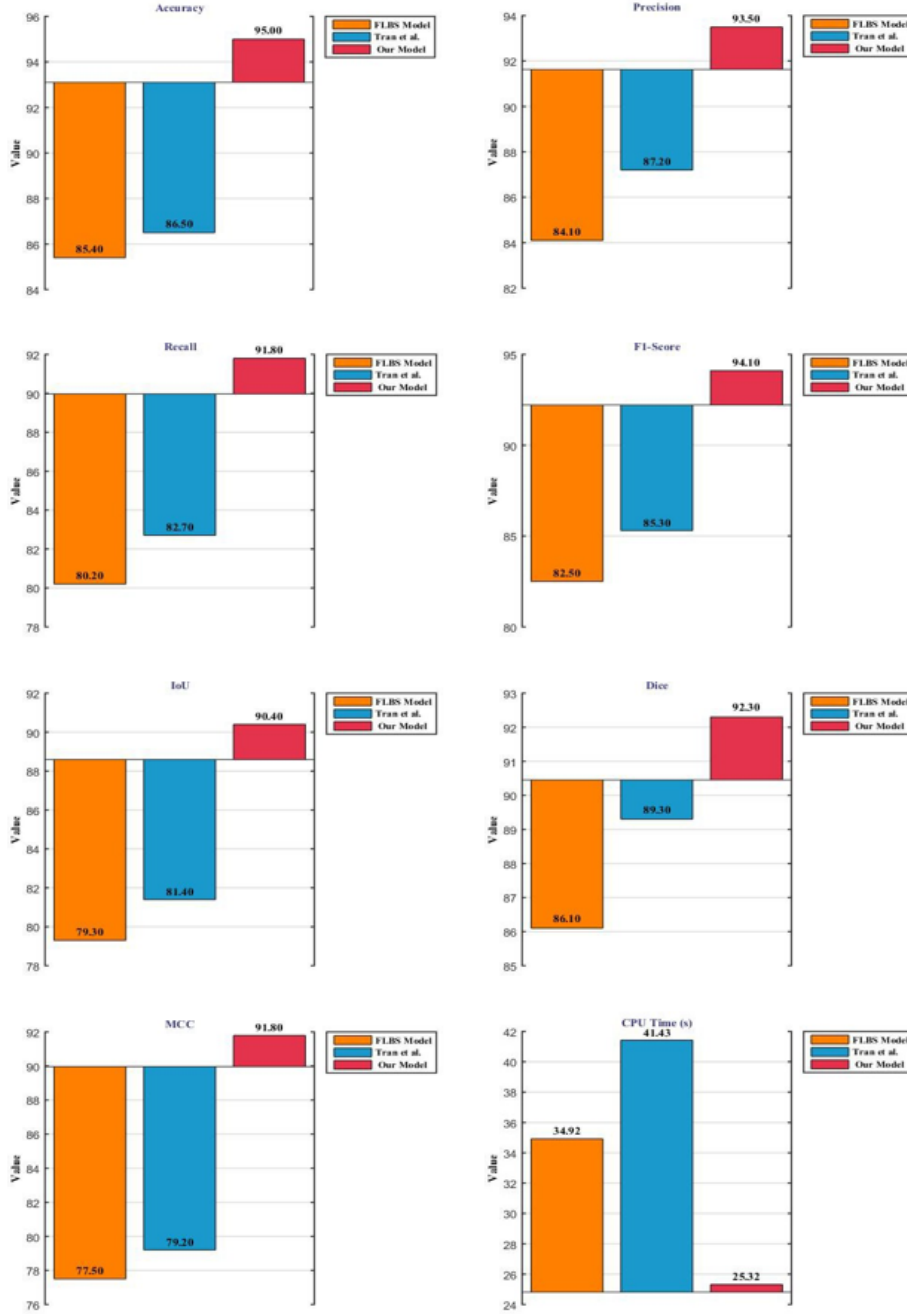


Figure 5. Comparative bar plots illustrating segmentation performance metrics, including accuracy, precision, recall, F1-score, IoU, Dice, MCC, and CPU execution time for the FLBS model, the approach developed by Tran et al. [25], and the proposed model

The results highlight the superior performance of the proposed model across all segmentation metrics. The proposed model achieves the highest accuracy (95.0%), precision (93.5%), and recall (91.8%), indicating its ability to accurately classify segmented regions while minimizing false positives and false negatives. Additionally, the F1-score (94.1%) and IoU (90.4%) demonstrate the model's effectiveness in achieving high-quality segmentation results with minimal overlap errors. The Dice coefficient (92.3%) and MCC (91.8%) further validate the robustness of the proposed method in maintaining segmentation consistency.

In contrast, the FLBS model and the approach developed by Tran et al. [25] struggle to achieve comparable performance. The FLBS model exhibits lower accuracy (85.4%) and recall (80.2%), indicating its difficulty in correctly identifying segmented regions, particularly in the presence of intensity inhomogeneity and noise. Similarly, the approach developed by Tran et al. [25], while slightly better than FLBS in some metrics, still underperforms in terms of segmentation reliability, achieving an accuracy of 86.5% and recall of 82.7%.

Apart from segmentation quality, computational efficiency is also a critical factor. The CPU time results indicate that the proposed model (25.32 s) is significantly faster than the FLBS model (34.92 s) and the approach developed by Tran et al. [25] (41.43 s). This efficiency advantage demonstrates that the proposed method not only improves segmentation accuracy but also reduces computational overhead, enhancing its applicability in practical, real-world scenarios.

Overall, these results confirm that the proposed model outperforms the competing methods in accuracy and all other efficiency, making it a more reliable and computationally efficient choice for segmentation tasks in complex imaging conditions (Figure 5). As shown in the figure, the performance of the proposed model surpasses that of all baseline methods, demonstrating superior results across every evaluation criterion, demonstrating superior segmentation accuracy and computational efficiency.

Table 1. Segmentation performance evaluation of the proposed and competing models

Metric	FLBS Model [24]	Approach Developed by Tran et al. [25]	Proposed Model
Accuracy	85.4	86.5	95.0
Precision	84.1	87.2	93.5
Recall	80.2	82.7	91.8
F1-score	82.5	85.3	94.1
IoU	79.3	81.4	90.4
Dice	86.1	89.3	92.3
MCC	77.5	79.2	91.8
CPU	34.92	41.43	25.32

5 Conclusion

In this study, a PyFS-based segmentation model was proposed, which effectively addressed intensity inhomogeneity and noise by integrating fuzzy membership-based local averaging and an adaptive energy functional. The model demonstrated robustness against noise, weak edges, and intensity variations, leading to improved segmentation accuracy in challenging imaging conditions. This approach has potential applications in medical imaging, remote sensing, and industrial defect detection. The code is available for research purposes upon request via email.

Despite its advantages, the proposed model has certain limitations. The integration of PyFSs requires iterative updates of membership functions, making the segmentation process computationally intensive, particularly for high-resolution images. Additionally, the performance depends on hyperparameter selection, such as fuzzy weighting coefficients and neighborhood size, which require fine-tuning for different datasets. Another limitation is the trade-off between edge preservation and smoothing, where the local averaging mechanism may slightly blur sharp edges, affecting fine boundary details.

Future research could focus on enhancing the multi-target segmentation capabilities of the proposed PyFS-based model by integrating attention mechanisms. Attention-based techniques can improve the model's ability to selectively focus on relevant image regions, thereby refining segmentation accuracy in complex scenes. Additionally, the integration of PyFSs with transformer networks and graph-based models could be explored to improve generalization across diverse imaging modalities. To further optimize computational efficiency, future work could also investigate advanced numerical solvers and automated parameter selection using machine learning techniques. These advancements aim to enhance the scalability and robustness of the proposed model for real-world applications.

Data Availability

The data used to support the research findings are available from the corresponding author upon request.

Conflicts of Interest

The author declares no conflict of interest.

References

- [1] I. Hussain and J. Muhammad, "Efficient convex region-based segmentation for noising and inhomogeneous patterns," *Inverse Probl. Imaging*, vol. 17, no. 3, pp. 708–725, 2023. <https://doi.org/10.3934/ipi.2022074>
- [2] S. Bouhafra and H. El Bahi, "Deep learning approaches for brain tumor detection and classification using MRI images (2020 to 2024): A systematic review," *J. Digit Imaging. Inform. Med.*, pp. 1–31, 2024. <https://doi.org/10.1007/s10278-024-01283-8>
- [3] A. K. M, A. Gladston, S. R. M, and G. N. S, "Agricultural leaf disease segmentation approaches using deep learning," in *2024 5th International Conference on Data Intelligence and Cognitive Informatics (ICDICI), Tirunelveli, India*, 2024, pp. 585–592. <https://doi.org/10.1109/ICDICI62993.2024.10810867>

- [4] I. Hussain, H. Ali, M. S. Khan, N. SIJIE, and L. Rada, “Robust region-based active contour models via local statistical similarity and local similarity factor for intensity inhomogeneity and high noise image segmentation,” *Inverse Probl. Imaging*, vol. 16, no. 5, p. 1113, 2022. <https://doi.org/10.3934/ipi.2022014>
- [5] M. A. Al-qaness, J. Zhu, D. AL-Alimi, A. Dahou, S. H. Alsamhi, M. Abd Elaziz, and A. A. Ewees, “Chest x-ray images for lung disease detection using deep learning techniques: A comprehensive survey,” *Arch. Comput. Methods Eng.*, vol. 31, no. 6, pp. 3267–3301, 2024. <https://doi.org/10.1007/s11831-024-10081-y>
- [6] Y. Wang and C. J. He, “Fractional guidance-based level set evolution for noisy image segmentation with intensity inhomogeneity,” *Appl. Math. Modell.*, vol. 130, pp. 580–602, 2024. <https://doi.org/10.1016/j.apm.2024.03.019>
- [7] M. S. Khan, “A region-based fuzzy logic approach for enhancing road image visibility in foggy conditions,” *Mechatron. Intell. Transp. Syst.*, vol. 3, no. 4, pp. 212–222, 2024. <https://doi.org/10.56578/mits030402>
- [8] J. Yang, S. Guo, M. J. Bocus, Q. Chen, and R. Fan, “Semantic segmentation for autonomous driving,” in *Autonomous Driving Perception: Fundamentals and Applications, Singapore*, 2023, pp. 101–137. https://doi.org/10.1007/978-981-99-4287-9_4
- [9] Z. Wang, X. Gao, R. Wu, J. Kang, and Y. Zhang, “Fully automatic image segmentation based on FCN and graph cuts,” *Multimed. Syst.*, vol. 28, pp. 1753–1765, 2022. <https://doi.org/10.1007/s00530-022-00945-3>
- [10] W. Wu, Z. He, M. Gao, S. Pu, X. Wu, Q. Wan, and Z. Chen, “Edge-preserving texture-based semantic segmentation for ultrahigh resolution images in agricultural scene,” *J. Indian Soc. Remote Sens.*, vol. 53, pp. 1037–1052, 2025. <https://doi.org/10.1007/s12524-024-02021-x>
- [11] S. Das, “Automated building segmentation in areal images using boundary edge detection,” in *International Conference on Advances in Data-driven Computing and Intelligent Systems, Singapore*, 2024, pp. 237–250. https://doi.org/10.1007/978-981-99-9518-9_17
- [12] B. K. Sa, R. Panda, and S. Agrawal, “Relevant edge probability-based adaptively weighted active contour for medical image segmentation,” *Int. J. Imaging Syst. Technol.*, vol. 34, no. 2, p. e22993, 2024. <https://doi.org/10.1002/ima.22993>
- [13] T. S. Arulananth, P. Chinnasamy, J. C. Babu, A. Kiran, J. Hemalatha, and M. Abbas, “Edge detection using fast pixel based matching and contours mapping algorithms,” *PLoS ONE*, vol. 18, no. 8, p. e0289823, 2023. <https://doi.org/10.1371/journal.pone.0289823>
- [14] M. Shi and I. Hussain, “Improved region-based active contour segmentation through divergence and convolution techniques,” *AIMS Math.*, vol. 10, no. 1, pp. 654–671, 2025. <https://doi.org/10.3934/math.2025029>
- [15] T. F. Chan and L. A. Vese, “Active contours without edges,” *IEEE Trans. Image Process.*, vol. 10, no. 2, pp. 266–277, 2001. <https://doi.org/10.1109/83.902291>
- [16] L. A. Vese and T. F. Chan, “A multiphase level set framework for image segmentation using the Mumford and Shah model,” *Int. J. Comput. Vision*, vol. 50, no. 3, pp. 271–293, 2002. <https://doi.org/10.1023/A:1020874308076>
- [17] Q. Chen, Y. Chen, Y. Huang, X. Xie, and L. Yang, “Region-based online selective examination for weakly supervised semantic segmentation,” *Inf. Fusion*, vol. 107, p. 102311, 2024. <https://doi.org/10.1016/j.inffus.2024.102311>
- [18] R. Ronfard, “Region-based strategies for active contour models,” *Int. J. Comput. Vision*, vol. 13, no. 2, pp. 229–251, 1994. <https://doi.org/10.1007/BF01427153>
- [19] S. Minaee, Y. Boykov, F. Porikli, A. Plaza, N. Kehtarnavaz, and D. Terzopoulos, “Image segmentation using deep learning: A survey,” *IEEE Trans. Pattern Anal. Mach. Intell.*, vol. 44, no. 7, pp. 3523–3542, 2021. <https://doi.org/10.1109/TPAMI.2021.3059968>
- [20] Y. Yu, C. Wang, Q. Fu, R. Kou, F. Huang, B. Yang, T. Yang, and M. Gao, “Techniques and challenges of image segmentation: A review,” *Electronics*, vol. 12, no. 5, p. 1199, 2023. <https://doi.org/10.3390/electronics12051199>
- [21] K. Zhang and D. Liu, “Customized segment anything model for medical image segmentation,” *arXiv preprint arXiv:2304.13785*, 2023. <https://doi.org/10.48550/arXiv.2304.13785>
- [22] Y. Liu, C. Jing, H. Li, M. Zhu, H. Chen, X. Wang, and C. Shen, “A simple image segmentation framework via in-context examples,” *arXiv preprint arXiv:2410.04842*, 2024. <https://doi.org/10.48550/arXiv.2410.04842>
- [23] O. Derevyanchuk, “Use of intelligent fuzzy image segmentation systems in the professional training of future specialists in engineering and pedagogical fields,” *Prof. Pedagogics*, vol. 1, no. 28, pp. 103–115, 2024. <https://doi.org/10.32835/2707-3092.2024.28.103-115>
- [24] N. Narasimham and K. Keshav Kumar, “Fuzzy logic-based system for brain tumour detection and classification,” *arXiv preprint arXiv:2401.14414*, 2024. <https://doi.org/10.48550/arXiv.2401.14414>
- [25] H. D. Tran, T. C. Phan, V. P. Nguyen, and A. C. Phan, “Automatic segmentation of masses on mammograms using fuzzy logic,” in *International Conference on Intelligent Systems and Data Science, Singapore*, 2025, pp. 69–82. https://doi.org/10.1007/978-981-97-9613-7_6